Chinese Chemical Letters 32 (2021) 1780–1784

Contents lists available at ScienceDirect

Chinese Chemical Letters

journal homepage: www.elsevier.com/locate/cclet

Communication

Self-assembled all-inclusive organic-inorganic nanoparticles enable cascade reaction for the detection of glucose

Ximei Sun[a], Yan Li[a], Qian Yang[b,**], Yunwei Xiao[c], Yuting Zeng[a], Jindi Gong[a], Ziyu Wang[a], Xiaofeng Tan[a,d,**], He Li[a,*]

[a] College of Optoelectronics Technology, Chengdu University of Information Technology, Chengdu 610225, China
[b] School of Pharmacy, Chengdu Medical College, Chengdu 610500, China
[c] Chengdu No. 7 High School, Chengdu 610041, China
[d] School of Chemistry and Chemical Engineering, University of Ji'nan, Ji'nan 250022, China

ARTICLE INFO

Article history:
Received 12 October 2020
Received in revised form 23 December 2020
Accepted 23 December 2020
Available online 25 December 2020

Keywords:
Self-assembly
All-inclusive nanoparticles
Glucose detection
Colorimetric and photothermal bioassay
Chromogenic substrates

ABSTRACT

Traditional colorimetric glucose biosensor generally involves complex assay procedures. Free labile enzymes and peroxidase substrates are used separately for triggering a chromogenic reaction. These limits result in inferior enzyme stability and defective enzymatic catalytic efficiency, making it hard to routinely utilize them for the direct and fast test of glucose. In this work, we provide an all-inclusive substrates/enzymes nanoparticle employed 3,3′5,5′-tetramethylbenzidine (TMB) as chromogenic substrates and glucose oxidase (GOx)/horseradish peroxidase (HRP) as signal amplifier enzymes (TMB-GH NPs) by the molecule self-assembly technique. The "all-inclusive" nanoparticles can realize the tandem colorimetric reactions, and the oxidation product of TMB (ox-TMB) exhibits a strong NIR laser-driven photothermal effect, thus allowing quantitative photothermal detection of glucose. Owing to the restriction of the molecular motion of GOx, HRP, and TMB, the distance of mass transfer between substrates was shortened largely, leading to improved catalytic activity for glucose. Overall, our strategy will simplify the analysis procedure, furthermore, these integrated nanoparticles not only display higher stability and activity than that of the free GOx/HRP system and possesses an excellent performance for colorimetric and photothermal bioassay of glucose simultaneously. We believe that this unique technique will give good inspirations to develop simple and precise methods for bioassay.

Diabetes has been an imperious global health issue. More than 425 million people are suffering from diabetes worldwide and over 4 million deaths in 2017, and a predicted 48% increase up to 629 million people who would have diabetes in 2045 [1,2]. Owing to being out of control on high blood glucose level, consequent further complications which are hardly remedied by pharmaceuticals torment the diabetic patients [3,4]. Therefore, the monitor and control of blood glucose levels for them is significantly critical to maintaining the quality of life. These motivate a widespread development of glucose biosensors with desirable reliability, admirable sensitivity and selectivity, low cost, and fast response [5–7].

Glucose biosensors utilize enzymes or nanozymes and substrates to generate easily-traced signals including color changes [8], fluorescence [9,10], chemiluminescence [11], and electrochemistry [12,13]. The colorimetric glucose biosensor, especially with regards to cascade glucose biosensor, has drawn considerable attention owing to its practicality, simplicity, and low cost [14–16]. The detection process is commonly divided into two procedures. The former involves the pre-incubation of glucose and glucose oxidase (GOx) to generate H_2O_2, the latter comprises a typical chromogenic reaction by the addition of horseradish peroxidase (HRP) or peroxidase-like nanomaterials and peroxidase substrates. The strategy covers very complex procedures, making it challenging to regularly employ them for the point-of-care test (POCT) [17–19]. In addition, the catalytic efficiency of the cascade reaction is limited drastically due to low diffusion ability and unstable intermediates [20]. Also, some integration nanomaterials with GOx-like and HRP-like activity simultaneously have been reported, thus improving the sensitivity and selectivity for glucose detection [21–23].

* Corresponding author.
** Corresponding author at: College of Optoelectronics Technology, Chengdu University of Information Technology, Chengdu 610225, China.
E-mail addresses: yoyoyoung8293@gmail.com (Q. Yang), tanxiaofengjndx@foxmail.com (X. Tan), lihecd@cuit.edu.cn (H. Li).

https://doi.org/10.1016/j.cclet.2020.12.041
1001-8417/

Recently, the molecule self-assembly technique in water is employed as the most efficient method of preparing carrier-free nanodrug in drug delivery systems [24–26]. Normally, the small hydrophobic drug molecules directly assembled into small nanoparticles (NPs) from soluble solutions into poor ones, accompanied by improved stability and dispersibility. Inspired by this, a common enzyme reaction substrate, 3,3′,5,5′-tetramethylbenzidine (TMB), dimethyl sulfoxide (DMSO)-soluble while entirely water-insoluble, is widely used in glucose colorimetric biosensing. The hydrophobic TMB molecules can self-assemble into well-defined NPs by the strong hydrophobic interactions and π-π stacking when it transfers from the DMSO solution into an aqueous one. The formed abundant amino groups on the surface of TMB NPs are beneficial to the enzyme absorption through hydrogen-bonding and van der Waals interactions [27].

Herein, we developed a simple TMB-GH NPs for the handy and rapid detection of glucose. The all-inclusive system contained all required components including GOx, HRP, and TMB NPs for glucose detection. The enzymes part as signal amplification units participated in the cascade catalysis reactions, which also functioned as stabilizing agents to improve the stability and dispersibility. Another part was activated in organic-inorganic reaction to produce the blue ox-TMB for colorimetric glucose biosensing. Moreover, the ox-TMB also can be functioned as a photothermal probe to convert the glucose concentrations into heat readout, which can be handily assessed using just a thermometer after 808 nm laser irradiation for sensitive photothermal glucose biosensing (Fig. 1). Owing to the restriction of the molecular motion of multi-enzymes and TMB, the *in situ* formed H_2O_2 generated by GOx and glucose can instantly be oxidized by HRP to elicit a chromogenic reaction, diminishing the effect of diffusion resistance and minimization of the decomposition of H_2O_2. Hence, the cascade glucose detection can be realized with only incubation of glucose and TMB-GH NPs. Additionally, to accelerate the decomposition of TMB NPs in glucose detection, a common surfactant, dodecyl trimethyl ammonium chloride (DTAC) was introduced into the detection system. The result indicated that the sensitivity and incubation time of our glucose biosensor was improved largely by the addition of DTAC. Finally, the TMB-GH NPs-based biosensor displayed a linear response range and low detection limit (LOD) (0.05−10 mmol/L with LOD of 0.012 mmol/L for colorimetric assay, 0.1−100 mmol/L with LOD of 0.028 mmol/L for photothermal assay). Furthermore, the all-inclusive system also offered effective colorimetric and photothermal assay in serum for glucose detection, indicating potential practicability for a clinical test.

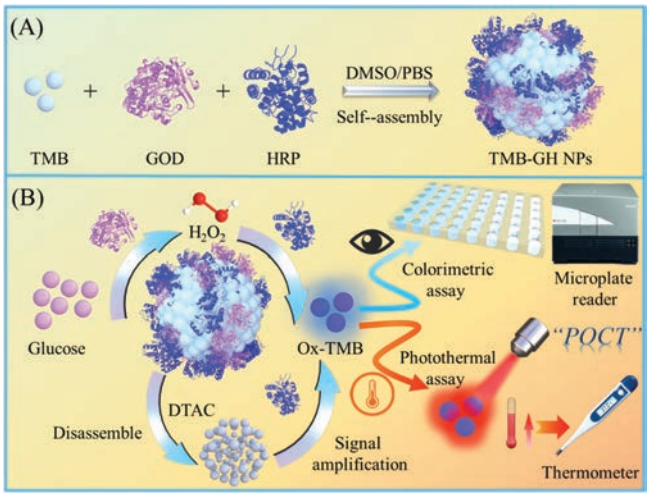

Fig. 1. Schematic illustration of the synthesis of TMB-GH NPs (A) and the corresponding detection principle for colorimetric and photothermal bioassay of glucose (B).

The preparation process of TMB-GH NPs was inspired by carrier-free nanodrug [28,29]. The hydrophobic TMB molecule can be self-assembled into well-defined nanoparticles owing to sudden environment change from the DMSO phase to the water phase. The enzymes containing in the aqueous phase were able to be immobilized within TMB NPs *via* hydrogen-bonding and van der Waals interactions. As revealed in Fig. 2A, uniform TMB-GH NPs with an average diameter of 110 nm were observed in transmission electron microscope (TEM) image. While TMB NPs without the participation of enzymes exhibited irregular morphology and were prone to be aggregated compared to enzymes-involved counterparts, demonstrating enhanced dispersity on nanoscale owing to the involvement of hydrophilic proteins (Fig. 2B). Fourier-transform infrared spectroscopy (FTIR) test was carried out to confirm the presence of GOx and HRP, evidenced by the characteristic bands at 1570–1680 cm^{-1} corresponding to the C=O stretching mode in TMB-GH NPs (Fig. 2C). To further verify the successful incorporation of GOx and HRP in TMB NPs, fluorescein isothiocyanate (FITC)-labeled GOx and rhodamine B (RhB)-labeled HRP were subjected to the same procedure to synthesize fluorescently labeled TMB-GH NPs. Confocal laser scanning microscopy (CLSM) images indicated that both FITC-GOx (green regions) and RhB-HRP (red regions) were dispersed homogeneously in TMB-GH NPs, revealing the incorporation of GOx and HRP in TMB-GH NPs (Figs. 2D–F). The dispersibility and stability of TMB-GH NPs were proved to be satisfactory. As shown in Fig. 2G, TMB molecules were largely water-insoluble and precipitated at the bottom of the bottle and TMB NPs became agglomerated while TMB-GH NPs exhibited better dispersibility and stability after 2 h, indicating enhanced dispersible stability by hydrophilic enzymes (Fig. 2H). The zeta potential measurements also reflected definite enzyme immobilization on TMB NPs owing to a shift in zeta potential value from −6.5 mV to −9.2 mV (Fig. 2I).

The feasibility of detection of glucose based on all-inclusive TMB-GH NPs was investigated. When TMB-GH NPs were incubated with glucose, the GOx converted glucose to gluconic acid and generates H_2O_2 which was the substrate for HRP oxidizing TMB to form oxidized products (ox-TMB), generating a noticeable blue color and absorption peak at 652 nm. It is noted that TMB-GH NPs were self-assembled through hydrogen-bonding and van der Waals interactions, and hardly disassembled to TMB molecules in the aqueous phase. To yield stronger color intensity, a typical surfactant, dodecyl trimethyl ammonium chloride (DTAC) was introduced into the system to break up TMB-GH NPs, the absorbance intensity has doubled than that without DTAC (Fig. 3A). As controls, TMB-GOx (TMB-G), TMB-HRP (TMB-H), and pure TMB NPs were synthesized and incubated with glucose and DTAC, no distinct peak was observed (Fig. 3B), suggesting only TMB-GH NPs possess tandem mimic enzyme activities for glucose. The self-carried TMB-GH NPs possess ultrahigh signal molecules loading capacities, which was estimated to be 748 mg/g by a standard absorbance curve (Fig. 3C), outperforming those of signal tag carrier-based nanomaterials [30–33] (Fig. 3D). The high loading capacity provided a more robust sensitivity for the detection of glucose. The loading amount of GOx and HRP on TMB-GH NPs was evaluated by a fluorescently labeled method. The FTIC-labeled GOx and RhB-labeled HRP were added into PBS and the relative intensity of them was measured to be 100%. After the preparation of TMB-GH NPs, the relative intensity of free GOx and HRP in supernatants was measured to be 89% and 87%, suggesting the overall 24% loading amount of enzymes approximately, which was in agreement with the result of TMB loading capacity (Fig. 3E).

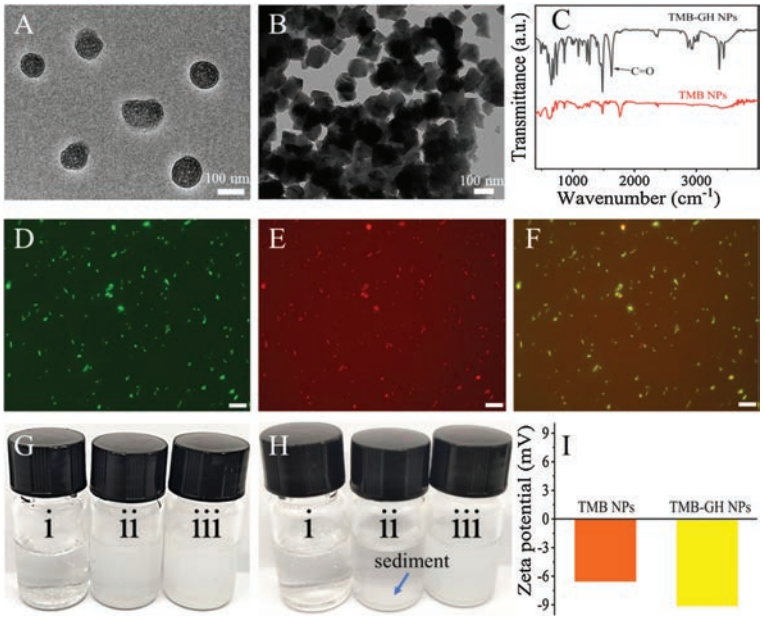

Fig. 2. TEM images of TMB-GH NPs (A) and individual TMB NPs (B). FTIR of TMB-GH NPs and TMB NPs (C). Confocal laser scanning microscopy images of fluorescently labeled TMB-GH NPs: GOx was labeled with FITC (green) (D) and HRP was labeled with RhB (red) (E) and their overlay image (F). Dispersibility of (i) TMB molecules, (ii) TMB NPs, (iii) TMB-GH NPs in PBS (G, fresh solution; H, after 2 h). Zeta potential of TMB NPs and TMB-GH NPs (I).

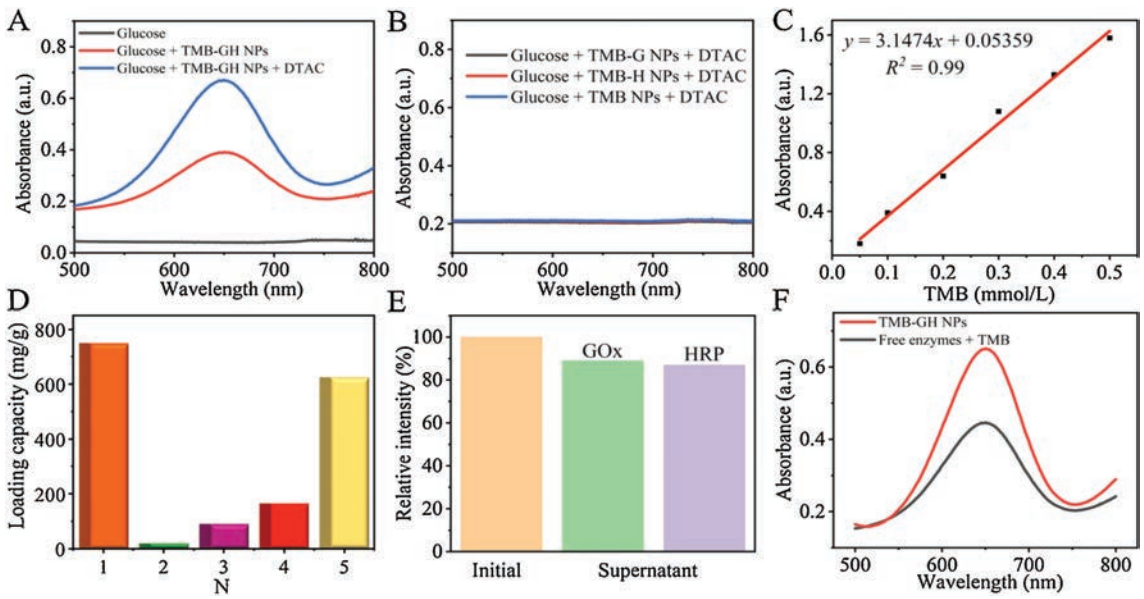

Fig. 3. UV–vis spectra of glucose, glucose + TMB-GH NPs, glucose + TMB-GH NPs + DTAC (A) and control groups, glucose + TMB-G/TMB-H/TMB NPs + DTAC (B). The standard curve of the TMB solution in DMSO (C). The comparisons of loading capacity with different carriers (D): (1) TMB-GH NPs, (2) mesoporous SiO_2-thymolphthalein [30], (3) C_3N_4 nanosheets-phenolphthalein [31], (4) polydopamine NPs-thymolphthalein [32], (5) MoS_2-curcumin [33]. The relative intensity of free GOx and HRP in the supernatant (E). The absorbance comparison of TMB-GH NPs and free enzymes with glucose under the same condition (F).

Then, the cascade catalytic performances of the integrated enzyme and free enzyme were compared. The results indicated that the absorbance of TMB-GH NPs was higher than that of free enzymes under the same condition (Fig. 3F). The all-inclusive TMB-GH NPs/glucose system fueled the great opportunity of shortening the distance of mass transport and minimize diffusion and self-decomposition of H_2O_2 for the chromogenic reaction.

The photothermal properties of TMB-GH NPs were also evaluated. An 808 nm laser at a power density of 1.86 W/cm^2 for 10 min was employed to test the photothermal effect of the colorimetric reaction system. As shown in Fig. S1A (Supporting information), the TMB-GH NPs/glucose system exhibited comparable temperature increase and reached its highest steady value after about 10 min. In contrast, TMB-GH NPs and pure water have no significant temperature increase, demonstrating that only TMB-GH NPs/glucose exhibited remarkable photothermal effect. This can be attributed to the yield of ox-TMB, which was a good photothermal agent. As controls, TMB-G NPs, TMB-H NPs, and pure TMB NPs have no tandem mimic enzyme activities for glucose and cannot induce the colorimetric reaction, thus no significant temperature increases were found (Fig. S1B in Supporting information).

For obtaining the ideal analytical performance, several crucial parameters including incubation time, DTAC concentration, and pH were optimized. First, the incubation time of the chromogenic reaction was investigated, and TMB-GH NPs/glucose system obtained a poor absorbance value and a long reaction time. For solving this issue, an additive, DTAC, was introduced into the system. TMB NPs were disassembled fast and oxidized entirely within 2 h, the absorbance values were higher than those of the control without DTAC (Fig. S2A in Supporting information). The DTAC concentration was also optimized. The absorbance gradually increased with the increasing DTAC concentration at the range of 0−4 mmol/L, and then reached a plateau after 4 mmol/L (Fig. S2B in Supporting information). The pH-dependent UV–vis absorbance raised with the increase of pH value then exhibited the strongest intensity at pH 4.0, and finally decreased beyond pH 4.0 (Fig. S2C in Supporting information). Therefore, the optimal incubation time, DTAC concentration, and pH were determined to be 2 h, 4 mmol/L, and 4.0, respectively.

The all-inclusive enzymes/TMB NPs system generated tandem enzymatic reactions for the quantitative detection of glucose. Under the optimal reaction conditions, TMB-GH NPs were incubated in HAc-NaAc buffer containing various concentrations of glucose (0.05−100 mmol/L) (Fig. 4A), then the absorbance at 652 nm was recorded. As expected, it exhibited a good linear relationship between the absorbance and the concentration of glucose ranging from 0.05−10 mmol/L with an R^2 value of 0.99 (Fig. 4B). The limit of detection (LOD) was determined to be 0.012 mmol/L (LOD value is calculated by $3\sigma/k$, σ denotes the standard deviation of the blank sample and k denotes the slope of the calibration curve). Then, the colorimetric reaction solutions were irradiated by an 808 nm laser for 10 min, respectively (Fig. 4C). The temperature elevation was linearly correlated with the logarithm of glucose concentrations and the calibration curve was established as to: ΔT (°C) = 11.2·Log*C*[glucose] (mmol/L) + 18.9 (R^2 = 0.96) in the range of 0.05 mmol/L to 100 mmol/L with a LOD of 0.028 mmol/L (Fig. 4D). Notably, the detection performances of TMB-GH NPs for glucose were superior to some reported glucose biosensor based on inorganic and enzyme-based nanomaterials [23,34–37] (Table S1 in Supporting information). The stability of TMB-GH NPs/glucose system was first examined. The results indicated that TMB-GH NPs/glucose system retained ~90% of initial overall activity even after 45 days, suggesting exceptional storage stability of enzymes within TMB-GH NPs (Fig. S3A in Supporting information). The reproducibility was investigated by measuring five same concentration of glucose simultaneously, the RSD of results were determined to be 4.1%, indicating a satisfactory reproducibility for glucose detection (Fig. S3B in Supporting information). The specific selectivity of TMB-GH NPs/glucose systems was inspected by comparing the absorbance at 652 nm with interfering carbohydrates, such as fructose, maltose, lactose, and sucrose with the same concentration (100 mmol/L). TMB-GH NPs/glucose system demonstrated a clear absorbance change at 652 nm, while other glucose analogues received a tiny absorbance increase even though their concentration was higher than that of glucose, signifying high specific selectivity for glucose detection (Fig. S3C in Supporting information).

To prove the practicability of the glucose biosensor, TMB-GH NPs were employed for detecting glucose levels in human serum samples. The consequent results are quite close to those detected by the glucometer, and relative standard deviations of them (RSD, n = 3) were less than 8% (Table S2 in Supporting information), indicating excellent accuracy and reliability of our glucose biosensor. Therefore, the prepared glucose sensing platform can be applied to human serum samples and possesses great potential for sensitive and convenient diagnostics. We are now carrying out the exploration of non-invasive blood glucose detection by integrating the all-inclusive TMB-GH NPs with a microneedle patch.

In summary, we prepared a new kind of all-inclusive TMB-GH NPs by the molecule self-assembly method. With the confinement of GOx, HRP, and TMB NPs, the dual-modal colorimetric and photothermal detection of glucose can be realized easily. The all-inclusive system enhanced the catalytic efficiency by shortening the distance between enzymes and substrates to diminish the

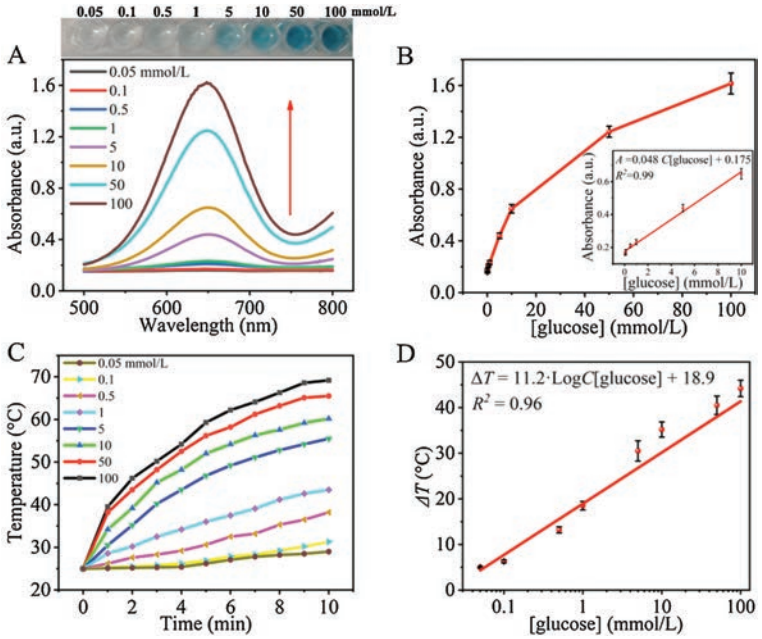

Fig. 4. UV–vis spectra (A) and corresponding photographs (A, top inset) upon addition of TMB-GH NPs in 0.05–100 mmol/L glucose. (B) A linear relationship between absorbance and a series of concentration of glucose based on TMB-GH NPs (0.05–10 mmol/L). (C) The temperature curves of ox-TMB solution for the detection of different glucose concentrations (0.05–100 mmol/L). (D) Calibration plots of the temperature increase (ΔT) *vs.* the logarithm of glucose concentration (mmol/L). The detection solutions (2 mL) were irradiated by the 808 nm laser for 10 min at a power density of 1.86 W/cm^2.

effect of diffusion resistance. Moreover, the integrated system decreases the number of steps for conventional analysis and makes glucose POCT assay more user-friendly. The TMB-GH NPs-based glucose biosensor exhibited a wide linear range (0.05−10 mmol/L for colorimetric method, 0.05−100 mmol/L for photothermal method) with a low limit of detection (0.012 mmol/L for colorimetric method, 0.028 mmol/L for photothermal method). The all-inclusive organic-inorganic NPs paved a new avenue for designing a novel integrated system for bioassay.

Declaration of competing interest

The authors report no declarations of interest.

Acknowledgments

The authors would like to thank the financial support from Sichuan Province Science and Technology Support Program (No. 2020YFN0029), the One-Thousand-Talents Scheme in Sichuan Province, Scientific Start-up Research Fund of Chengdu University of Information Technology (No. KYTZ201714). The human serum samples were kindly provided by Qilu Hospital of Shandong University. The authors would like to thank Shiyanjia Lab (www.shiyanjia.com) for the support of TEM test.

Appendix A. Supplementary data

Supplementary material related to this article can be found, in the online version, at doi:https://doi.org/10.1016/j.cclet.2020.12.041.

References

[1] J.J. Noubiap, J.R. Nansseu, U.F. Nyaga, et al., Lancet Glob. Health 7 (2019) e448–e460.
[2] L.P. Zhao, F. Zhang, X.Y. Ding, et al., Science 359 (2018) 1151–1156.
[3] E. Ahlqvist, N.R. Van Zuydam, L.C. Groop, M.I. McCarthy, Nat. Rev. Nephrol. 11 (2015) 277–287.
[4] C.M.O. Volpe, P.H. Villar-Delfino, P.M.F. dos Anjos, J.A. Nogueira-Machado, Cell Death Dis. 9 (2018) 1–9.
[5] D.L. Huang, X.G. Liu, C. Lai, et al., TrAC Trends Anal. Chem. 109 (2018) 260–274.
[6] X.G. Liu, D.L. Huang, C. Lai, et al., Small 15 (2019) 1900133.
[7] L. Jiao, W.Q. Xu, H.Y. Yan, et al., Chem. Commun. 55 (2019) 9865–9868.
[8] L.H. Jin, Z. Meng, Y.Q. Zhang, et al., ACS Appl. Mater. Interfaces 9 (2017) 10027–10033.
[9] L.Y. Chen, W.H. Tse, Y. Chen, et al., Biosens. Bioelectron. 91 (2017) 393–399.
[10] M. Hu, J. Qi, J. Ruan, G. Shen, J. Biomed. Nanotechnol. 14 (2018) 1117–1124.
[11] M.J. Chaichi, M. Ehsani, Sens. Actuators B: Chem. 223 (2016) 713–722.
[12] O. Parlak, A. İncel, L. Uzun, et al., Biosens. Bioelectron. 89 (2017) 545–550.
[13] X. Lin, Y. Wang, M. Zou, et al., Chin. Chem. Lett. 30 (2019) 1157–1160.
[14] L. Han, H.J. Zhang, D.Y. Chen, F. Li, Adv. Funct. Mater. 28 (2018) 1800018.
[15] H.J. Zhang, X. Liang, L. Han, F. Li, Small 14 (2018) 1803256.
[16] L.L. Zhang, J. Pan, Y. Long, et al., Small (2019) 1903182.
[17] C. Wu, H.H. Sun, Y.F. Li, et al., Biosens. Bioelectron. 66 (2015) 350–355.
[18] Q.Q. Wang, X.P. Zhang, L. Huang, et al., Angew. Chem. Int. Ed. 56 (2017) 16082–16085.
[19] Y.M. Xiong, Y.Y. Zhang, P.F. Rong, et al., Nanoscale 7 (2015) 15584–15588.
[20] W.Q. Xu, L. Jiao, H.Y. Yan, et al., ACS Appl. Mater. Interfaces 11 (2019) 22096–22101.
[21] J. Guo, Y. Wang, M. Zhao, Sens. Actuators B: Chem. 284 (2019) 45–54.
[22] L. Han, H. Zhang, D. Chen, F. Li, Adv. Funct. Mater. 28 (2018) 1800018.
[23] M. Liu, Z. Li, Y. Li, et al., Chin. Chem. Lett. 30 (2019) 1009–1012.
[24] S. Cheung, D.F. O'Shea, Nat. Commun. 8 (2017) 1885.
[25] N. Zhang, M.H. Li, X.T. Sun, et al., Biomaterials 159 (2018) 25–36.
[26] P.P. Liang, X.Y. Huang, Y. Wang, et al., ACS Nano 12 (2018) 11446–11457.
[27] L. Jiao, H.Y. Yan, W.Q. Xu, et al., Anal. Chem. 91 (2019) 8461–8465.
[28] X.L. Wu, J. Ge, C. Yang, et al., Chem. Commun. 51 (2015) 13408–13411.
[29] V. Krishnan, A. Sarode, R. Bhatt, et al., Adv. Ther. 1 (2018) 1800010.
[30] F.Y. Shao, L.H. Zhang, L. Jiao, et al., Anal. Chem. 90 (2018) 8673–8679.
[31] F.Y. Shao, L. Jiao, L.Y. Miao, et al., Biosens. Bioelectron. 90 (2017) 1–5.
[32] L. Jiao, Z.Y. Xu, W.W. Du, et al., ACS Appl. Mater. Interfaces 9 (2017) 28339–28345.
[33] L.Y. Miao, C.Z. Zhu, L. Jiao, et al., Anal. Chem. 90 (2018) 1976–1982.
[34] J. Xu, K. Xu, Y. Han, et al., Analyst 145 (2020) 5141–5147.
[35] Y.C. Yee, R. Hashim, A.R. Mohd Yahya, Y. Bustami, Sensors 19 (2019) 2511.
[36] Y.P. Li, L. Jiang, T. Zhang, et al., Chin. Chem. Lett. 25 (2014) 77–79.
[37] A. Liu, M. Li, J. Wang, et al., Chin. Chem. Lett. 31 (2020) 1133–1136.